ITU Journal of Metallurgy and Materials Engineering

ITU/MMEJ

Computational Investigation of the Effect of Manganese Substitution on the Mechanical Properties of $AlCr_2B_2$

Ahmet Sefa Atalay [1,2], Bora Derin [1]

[1] Istanbul Technical University, Department of Metallurgical and Materials Engineering, 34469, Maslak, Istanbul, Turkey.
[2] Kocaeli University, Department of Machine and Metal Technology, 41180, Kocaeli, Turkey.

Abstract: $AlCr_2B_2$ stands out with its superior mechanical properties compared to other ternary transition metal diboride MAB phases. In this study, the current chromium (Cr) content in $AlCr_2B_2$ compound has been reduced by 50%, and manganese (Mn) has been added in place of the reduced chromium. Using density functional theory (DFT)-based first-principles calculations, the effect of the added manganese on the mechanical properties has been investigated. The mechanical stabilities, elastic constants, elastic moduli (bulk modulus, shear modulus, and Young's modulus), Poisson ratios, Pugh ratios, theoretical Vickers hardness, Cauchy pressures, elastic anisotropies, and elastic Debye temperatures of $AlCr_{(2-x)}Mn_xB_2$ compounds have been studied for x values of 0 and 1. Both $AlCr_2B_2$ and $AlCrMnB_2$ compounds have been considered mechanically stable as they satisfy stability criteria. It has been observed that the elastic moduli, hardness, and elastic anisotropy of $AlCr_2B_2$ compound are slightly greater than those of the $AlCrMnB_2$ compound. Therefore, the addition of manganese as the fourth alloying element has been found to decrease stiffness and hardness while increasing isotropy.

Keywords: $AlCr_2B_2$, first-principles calculations, mechanical properties.

Mangan İkamesinin $AlCr_2B_2$'nin Mekanik Özellikleri Üzerindeki Etkisinin Hesaplamalı Olarak İncelenmesi

Özet: $AlCr_2B_2$, diğer üçlü geçiş metal diborür MAB fazlarıyla karşılaştırıldığında üstün mekanik özellikleriyle öne çıkmaktadır. Bu çalışmada, $AlCr_2B_2$ bileşiğindeki mevcut krom (Cr) miktarı %50 azaltılmış ve azaltılan kromun yerine mangan (Mn) eklenmiştir. Yoğunluk fonksiyonel teorisi (YFT) temelli ilk prensiplere dayalı hesaplamalar kullanılarak, mekanik özellikler üzerinde eksiltilen kromun yerine eklenen manganın etkisi araştırılmıştır. $AlCr_{(2-x)}Mn_xB_2$ bileşiklerinin mekanik stabiliteleri, elastik sabitleri, elastik modülleri (hacim modülü, kayma modülü ve Young modülü), Poisson oranları, Pugh oranları, teorik Vickers sertlikleri, Cauchy basınçları, elastik anizotropileri ve elastik Debye sıcaklıkları üzerine yapılan araştırma, x'in 0 ve 1 değerleri için gerçekleştirilmiştir. Hem $AlCr_2B_2$ hem de $AlCrMnB_2$ bileşikleri mekanik stabilite kriterlerini sağladıkları için mekanik olarak stabil kabul edilmiştir. $AlCr_2B_2$ bileşiğinin elastik modülleri, sertliği ve elastik anizotropisi $AlCrMnB_2$ bileşiğinden biraz daha büyük olduğu görülmüştür. Bu sebeple, manganın dördüncü alaşım elementi olarak eklenmesi, rijitliği ve sertliği azaltırken izotropiyi arttırdığı sonucu ortaya çıkmıştır.

Anahtar Kelimeler: $AlCr_2B_2$, ilk prensiplere dayalı hesaplamalar, mekanik özellikler.

Article

Corresponding Author: Ahmet Sefa Atalay[1], Bora Derin[2], E-mail: atalaya17@itu.edu.tr[1], ahmet.atalay@kocaeli.edu.tr[1], bderin@itu.edu.tr[2]

Reference: Atalay, A.S.,& Derin, B. (2024). Computational investigation of the effect of manganese substitution on the mechanical properties of $AlCr_2B_2$. *ITU Journal of Metallurgy and Materials Engineering, 1(1),* 1-6.

Submission Date: 28 February 2024
Online Acceptance : 23 July 2024
Online Publishing :26 July 2024

1.Introduction

Transition metal borides (TMBs) have garnered significant interest due to their remarkable properties (Wang et al. 2018; Zhu et al. 2019). They possess exceptional hardness values and boast high melting points, making them highly durable materials (Kota et al., 2020; Han et al. 2015; Wang et al. 2018; Zhu et al., 2019). Moreover, they demonstrate outstanding performance even in extremely high-temperature conditions (Lu et al. 2017; Verger et al., 2018). Additionally, these borides exhibit good thermal and electrical conductivities, further enhancing their appeal for various applications (Verger et al., 2018; Kota et al., 2020). These materials hold great promise in various industrial and technological fields due to their unique combination of desirable properties (Chai et al., 2015; Aydin and Şimşek, 2020; Kota et al., 2020). The MAB phases belong to a category of ternary transition metal borides with an atomically laminated structure. The MAB phases closely resemble well-known MAX phases, which are composed of the introduction of A-group elements into binary carbides or nitrides. Within MAB phases, the metal boride (M-B) layers consist of face-sharing BM_6 trigonal prisms, and they are separated by a monolayer or bilayers of Al atoms. The boron (B) atoms are closely spaced, forming covalently bonded "zig-zag" chains (Natu et al., 2020). Among the known $AlTM_2B_2$ (TM= Fe, Cr, Mn) MAB phases, the $AlCr_2B_2$ is particularly remarkable for its stiffness. Compared to other similar MAB phases, $AlCr_2B_2$ has remarkable stiffness; however, the situation is opposite in terms of ductility and elasticity (Kádas et al., 2017). The stiffness of materials is described using Young's modulus, and a higher Young's modulus indicates a greater level of stiffness in the material (Peng et al., 2022). In the studies that utilized first-principles calculations based on Density Functional Theory (DFT) for $AlCr_2B_2$, Young's modulus (E) was determined by computing elastic stiffness constants (C_{ij}) independently by M. M. Ali et al. (Ali et al., 2020), X. H. Li et al. (Li, Cui, and Zhang 2018), K. Kadas et al. (Kádas et al., 2017), and L. Nie et al. (Nie et al., 2013).

The main purpose of this work is to conduct a comprehensive study using first-principles calculations based on DFT to investigate the influence of adding the Mn element, instead of the subtracted Cr element, on the mechanical properties of the $AlCr_2B_2$. Additionally, due to the high brittleness of the $AlCr_2B_2$, the addition of Mn as the fourth alloying element aims to increase the boride's ductility and improve its elasticity.

2. Materials and Methods

The mechanical properties of $AlCr_{(2-x)}Mn_xB_2$ (x= 0, 1) compounds were studied using the **CA**mbridge **S**equential **T**otal **E**nergy **P**ackage (CASTEP) code, employing the pseudo-potential based plane wave density functional theory (DFT) method (Clark et al., 2005). The Perdew-Burke-Ernzerhof (PBE) functional, a part of the Generalized Gradient Approximation (GGA), was employed as the exchange-correlation potential. In the context of the calculation method, the interaction between electrons and ion cores is handled in reciprocal space through the utilization of ultrasoft pseudopotentials (Ali et al., 2020). The Brillouin zone was sampled using the Monkhorst-Pack scheme, which involves dividing the reciprocal lattice into a set of discrete k-points (Monkhorst and Pack, 1976). The energy cutoff and the number of k-points were systematically increased until the calculated total energy reached the required level of convergence within a specified tolerance, typically set as a total energy difference of less than 1 millielectronvolt (meV). After convergence, the optimal cutoff energy of 600 eV and k-point grids with mesh parameters of 8 x 8 x 8 and 10 x 10 x 10, respectively, were selected to calculate the equilibrium lattice parameter for $AlCr_2B_2$ and $AlCrMnB_2$ materials.

$AlCr_2B_2$ crystallizes in an orthorhombic lattice with space group *Cmmm* (No. 65) and lattice constants a= 2.921, b= 11.036, c= 2.931 (Nie et al., 2013; Ali et al., 2020). The crystal structure of $AlCr_2B_2$ consists of Cr atoms located at the 4j site (0, 0.352, 0.5), Al atom at the 2a site (0, 0, 0), and B atoms at the 4i site (0, 0.22, 0) (Nie et al., 2013). For Mn as the fourth alloying element to be added instead of the Cr atoms removed from the $AlCr_2B_2$ crystal structure, the unit cell of the $AlCr_2B_2$ crystal lattice was transformed into a super-lattice. A novel crystal structure was created by replacing 50% of the Cr atoms in the $AlCr_2B_2$ with the fourth alloying element Mn. The borides $AlCr_2B_2$ and $AlCrMnB_2$ were visualized using open-source **V**isualization for **E**lectronic and **ST**ructural **A**nalysis (VESTA) (Momma and Izumi, 2011). Crystal structures of borides as shown in Figure 1.

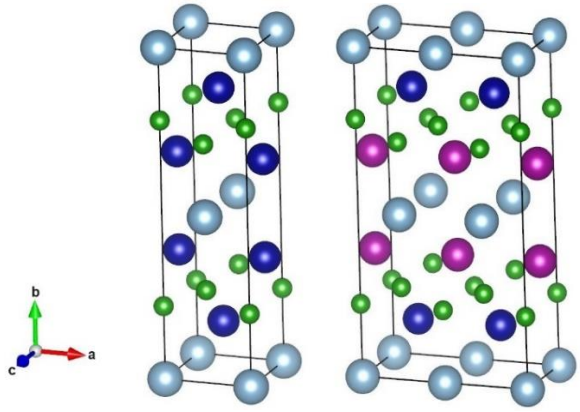

$AlCr_2B_2$ **$AlCrMnB_2$**

Figure 1. Crystal structures of $AlCr_2B_2$ and $AlCrMnB_2$. The unit cells are shown by black lines. Al, Cr, B, and Mn atoms are displayed in blue, navy blue, green, and purple respectively.
Şekil 1. $AlCr_2B_2$ ve $AlCrMnB_2$'nin kristal yapıları. Birim hücreler siyah çizgilerle gösterilmiştir. Al, Cr, B ve Mn atomları sırasıyla mavi, lacivert, yeşil ve mor renklerle gösterilmiştir.

3. Results and Discussion

In this study, the elastic constants of $AlCr_{(2-x)}Mn_xB_2$ (x= 0, 1) compounds with an orthorhombic crystal structure were calculated using the CASTEP code. Geometric optimization was performed on the crystal structures of $AlCr_2B_2$ and $AlCrMnB_2$ before calculating the elastic constants. Optimized lattice parameters of borides are given in Table 1.

Table 1. Optimized lattice parameters (a, b, c) and unit cell volume (V) of $AlCr_2B_2$ and $AlCrMnB_2$.
Tablo 1. $AlCr_2B_2$ ve $AlCrMnB_2$'nin optimize edilmiş kafes parametreleri (a, b, c) ve birim hücre hacmi (V).

Boride	a [Å]	b [Å]	c [Å]	V [Å^3]
$AlCr_2B_2$	2.923	11.041	2.934	94.688
$AlCrMnB_2$	5.791	10.984	2.924	185.990

As a result of the calculations, values such as the bulk modulus (B), shear modulus (G) and elastic Debye temperature (Θ) in addition to the elastic constants of the borides, have been obtained. In a material with an orthorhombic crystal structure, there are nine independent elastic constants: C_{11}, C_{22}, C_{33}, C_{44}, C_{55}, C_{66}, C_{12}, C_{13}, and C_{23} (Zhu et al., 2019). The calculated elastic constants of $AlCr_2B_2$ and $AlCrMnB_2$ are given in Table 2.

Table 2. Calculated elastic constants of $AlCr_2B_2$ and $AlCrMnB_2$.
Tablo 2. $AlCr_2B_2$ ve $AlCrMnB_2$'nin hesaplanan elastik sabitleri.

Boride	C_{11}	C_{22}	C_{33}	C_{44}	C_{55}	C_{66}	C_{12}	C_{13}	C_{23}
$AlCr_2B_2$	483.5	405.1	401.3	176.2	225.2	161.1	90.4	108.1	88.5
Ref. (Ali et al., 2020)	525	417	390	165	216	163	103	85	85
Ref. (Li et al., 2018)	457	397	414	156	199	164	89	89	100
$AlCrMnB_2$	479.4	392.4	428.7	157.9	210.4	172.6	86.4	106.5	86.1

For an orthorhombic crystal, the criteria for mechanical stability are $C_{11} > 0$, $C_{22} > 0$, $C_{33} > 0$, $C_{44} > 0$, $C_{55} > 0$, $C_{66} > 0$, $(C_{11} + C_{22} - 2C_{12}) > 0$, $(C_{22} + C_{33} - 2C_{13}) > 0$, $[C_{11} + C_{22} + C_{33} + 2(C_{12} + C_{13} + C_{23})] > 0$ (Wang et al., 2020). The borides $AlCr_2B_2$ and $AlCrMnB_2$ fulfill these stability criteria, indicating that they are mechanically stable. In all borides, it is observed that the elastic constant C_{11} is greater than the elastic constants C_{22} and C_{33}. This situation implies that all crystals will exhibit greater hardness against compression along the a-axis than compression along the b or c-axis. Therefore, it is considered that strong B-B bonds can exist along the a-axis in all crystals. The elastic constants C_{11} and C_{22} of the $AlCr_2B_2$ are larger than those of the $AlCrMnB_2$, but the elastic constant C_{33} is smaller. Therefore, the $AlCr_2B_2$ is expected to exhibit higher resistance to the compression applied in the a and b-axis compared to the $AlCrMnB_2$. Conversely, it is expected to have lower resistance to the compression applied in the c-axis.

After determining the single crystal elastic constants, we calculated the polycrystalline elastic constants, specifically the bulk moduli (B) and shear moduli (G), using two approximations: the Voigt (B_V, G_V) and Reuss (B_R, G_R) bounds. These bounds correspond to the upper and lower limits of the elastic moduli, respectively. Subsequently, Hill's bulk (B_H) and shear moduli (G_H) were obtained by calculating the average of the Voigt and Reuss bounds using the formulas: $B_H = (B_V + B_R) / 2$ and $G_H = (G_V + G_R) / 2$. The Young's modulus (E) and Poisson ratio (v) for an isotropic material are then

$$E_H = \frac{9B_H G_H}{G_H + 3B_H} \quad (1)$$

$$V_H = \frac{3B_H - 2G_H}{2(3B_H + G_H)} \quad (2)$$

The B/G ratio, also referred to as the Pugh ratio, which signifies the correlation between bulk and shear moduli, plays a pivotal role in assessing a material's elasticity and is employed to characterize the deformation behavior of a crystal. Materials that possess a ratio of B/G less than 1.75 are anticipated to exhibit brittleness, whereas materials with a B/G ratio exceeding 1.75 are likely to display ductile behavior (Kádas et al., 2017).The hardness of $AlCr_2B_2$ and $AlCrMnB_2$ was estimated using the relationship:

$$H_v = 2 \times \left({G_H}^3/{B_H}^2\right)^{0.585} - 3 \quad (3)$$

The bulk modulus (B_H) of the $AlCr_2B_2$ is slightly larger than that of the $AlCrMnB_2$. Therefore, it can be understood that the compressibility of the $AlCrMnB_2$ is higher. The Young's modulus (E) of the $AlCr_2B_2$ is greater than that of the $AlCrMnB_2$, which is why the $AlCr_2B_2$ has higher resistance to deformation. Similarly, it has been determined that the $AlCr_2B_2$ is harder than the $AlCrMnB_2$. It has been determined that in both borides, Pugh ratios are less than 1.75, indicating that they are brittle.

The $AlCr_2B_2$ is more brittle than the $AlCrMnB_2$ because it has a smaller Pugh ratio. The Poisson ratio value is the same (0.17) in both borides. Furthermore, having a Poisson ratio value of less than 0.26 supports the conclusion that they are brittle (Zhu et al., 2019). Moreover, due to Poisson's ratio values of borides being between -1 and 0.5, they are expected to remain stable under the influence of shear deformation (Ali et al., 2020). The Debye temperature is a crucial factor for metallic materials, as both interatomic force and thermal conductivity increase with its rise (Peng et al., 2022). The Debye temperature of the $AlCr_2B_2$ is higher than that of the $AlCrMnB_2$, hence the interatomic bonding strength of the $AlCr_2B_2$ is greater.
Table 3 presents the calculated values for the bulk modulus (B), shear modulus (G), Young's modulus (E), Poisson's ratio (v), Pugh ratio (B_H/G_H), hardness (H_V), and elastic Debye temperature (Θ) of both $AlCr_2B_2$ and $AlCrMnB_2$ materials.

Table 3. Calculated values of elastic modulus (B, G, and E) (in GPa), Poisson's ratio (v), Pugh ratio (B/G), Vickers hardness (H_V) (in GPa), and Debye temperature (Θ) (in Kelvin) for $AlCr_2B_2$ and $AlCrMnB_2$.
Tablo 3. $AlCr_2B_2$ ve $AlCrMnB_2$ için elastik modül (B, G ve E) (GPa cinsinden), Poisson oranı (v), Pugh oranı (B/G), Vickers sertliği (HV) (GPa cinsinden) ve Debye sıcaklığının (Θ) (Kelvin cinsinden) hesaplanan değerleri.

Boride	B_H	G_H	E	v	B_H/G_H	H_V	Θ
$AlCr_2B_2$	206.2	177.7	414.2	0.17	1.16	31.8	889.6
Ref. (Ali et al., 2020)	205	178	414	0.17	1.16	-	891
Ref. (Li et al., 2018)	202	169	397	0.17	-	29.6	-
$AlCrMnB_2$	205.6	175.3	409.4	0.17	1.17	31.1	873.7

In orthorhombic structures, the Cauchy pressure can be defined for the three different directions: $P_a = C_{23} - C_{44}$, $P_b = C_{13} - C_{55}$, and $P_c = C_{12} - C_{66}$. Generally, a positive Cauchy pressure indicates ductile behavior. In both borides, negative Cauchy pressures are observed in three directions, and this indicates that the borides are brittle (Kádas et al., 2017). The Cauchy pressures of the $AlCr_2B_2$ and $AlCrMnB_2$ are given in Table 4.

Table 4. The calculated Cauchy pressures of the $AlCr_2B_2$ and $AlCrMnB_2$.
Tablo 4. $AlCr_2B_2$ ve $AlCrMnB_2$'nin hesaplanan Cauchy basınçları.

Boride	P_a	P_b	P_c
$AlCr_2B_2$	-87.69	-117.09	-70.69
Ref. (Kádas et al., 2017)	-50.99	-87.99	-71.71
$AlCrMnB_2$	-71.87	-103.93	-86.27

In order to enhance the comprehension of the mechanical properties exhibited by $AlCr_2B_2$ and $AlCrMnB_2$, our investigation will focus on the analysis of their anisotropy. The elastic anisotropy of crystals is closely linked to anisotropic plastic deformation, as well as the generation and propagation of micro-cracks in materials (Nie et al., 2013; Peng et al., 2022). Therefore, discussing the elastic anisotropy of solids is crucial, and employing three indexes, including the universal elastic anisotropy index A^U, enhances the description of this phenomenon. Taking compression and shear effects into account, anisotropy can also be expressed as either $A_B = (B_V - B_R)/(B_V + B_R)$ or $A_G = (G_V - G_R)/(G_V + G_R)$, where B and G denote the bulk and shear moduli, respectively, and subscripts V and R refer to the Voigt and Reuss bounds, with A_B and A_G

values ranging from 0 to 1, corresponding to isotropy and the highest level of anisotropy, respectively (Wang et al., 2020). We used the universal elastic anisotropy index, A^U, in conjunction with the percentage indexes, A_G and A_B, and the calculation formula was as follows:

$$A^U = 5\frac{G_V}{G_R} + \frac{B_V}{B_R} - 6 \quad (4)$$

If $A^U = 0$ and $A_B = A_G = 0$, it indicates that the crystalline materials are isotropic in all directions otherwise anisotropic. The degree of anisotropy relies on the extent to which A^U deviates from zero. The greater the deviation from 0, the higher the degree of elastic anisotropy (Peng et al., 2022). The shear anisotropic factors measure the extent of anisotropy in the bonding between atoms in distinct planes and it can be calculated by

$$A_1 = \frac{4C_{44}}{C_{11}+C_{33}-2C_{13}} \quad (5)$$

for the {1 0 0} shear planes in <011> and <010> direction

$$A_2 = \frac{4C_{55}}{C_{22}+C_{33}-2C_{23}} \quad (6)$$

for the {0 1 0} shear planes in <101> and <001> directions and,

$$A_3 = \frac{4C_{66}}{C_{11}+C_{22}-2C_{12}} \quad (7)$$

for the {0 0 1} shear planes in <110> and <010> directions (Nie et al., 2013).

If A_1, A_2, and A_3 are all equal to 1, the solid is isotropic; otherwise, it is anisotropic (Zhu et al., 2019; Kádas et al., 2017). Both the A_1, A_2, and A_3 values of both $AlCr_2B_2$ and $AlCrMnB_2$ are not equal to 1, indicating that these borides are anisotropic. $AlCr_2B_2$ exhibits the highest anisotropy on the (010) plane. The universal elastic anisotropy index (A^U) accurately represents the anisotropy of a crystal since it arises from both bulk (A_B) and shear (A_G) anisotropy factors. In both borides, the fact that the A^U is not equal to zero supports the conclusion that the borides are anisotropic (Kádas et al., 2017; Peng et al., 2022; Zhu et al. 2019). Due to its A^U value being closest to zero, the $AlCrMnB_2$ has the lowest anisotropy. Table 5 presents the values of the parameters A_B, A_G, A^U, A_1, A_2, and A_3, which were determined to characterize the anisotropic properties of the $AlCr_2B_2$ and $AlCrMnB_2$.

Table 5. The calculated shear anisotropic factors (A_1, A_2, A_3), percentage anisotropy in compressibility A_B (%), percentage anisotropy in shear A_G (%), universal elastic anisotropy A^U of $AlCr_2B_2$ and $AlCrMnB_2$.
Tablo 5. $AlCr_2B_2$ ve $AlCrMnB_2$'nin hesaplanan kayma anizotropi faktörleri (A_1, A_2, A_3), sıkıştırılabilirlikteki yüzde anizotropi A_B (%), kaymadaki yüzde anizotropi A_G (%), evrensel anizotropi indeksi A^U.

Boride	A_1	A_2	A_3	A_B	A_G	A^U
$AlCr_2B_2$	1.05	1.43	0.91	0.43	0.91	0.10
Ref. (Kádas et al., 2017)	1.04	1.30	0.98	0.08	0.40	0.04
Ref. (Nie et al., 2013)	1.095	1.358	1.001	0.232	0.649	-
$AlCrMnB_2$	0.91	1.30	0.99	0.45	0.60	0.07

The values of elastic anisotropy indices are supported by the three-dimensional representations of directional Young's moduli and the two-dimensional representations of Young's moduli in the (100), (010), and (001) planes. The open-source software package AnisoVis was utilized for visualizing the anisotropic behavior of Young's moduli in various crystal planes in both two-dimensional (2D) and three-dimensional (3D) settings (Healy, 2023). In three-dimensional representations of directional Young's modulus, the degree of anisotropy is represented by the extent of deviation of the sphere (Peng et al., 2022; Zhu et al., 2019). When we examine the three-dimensional representations of direction-dependent Young's moduli, it is observed that in comparison to the $AlCrMnB_2$, the $AlCr_2B_2$ exhibits slightly more deviation from sphericity. The reason for this situation is due to the greater difference between the C_{11}-C_{33} elastic constants in $AlCr_2B_2$ (82.2) compared to $AlCrMnB_2$ (50.7). The three-dimensional representations of direction-dependent Young's moduli of the borides are given in Figure 2.

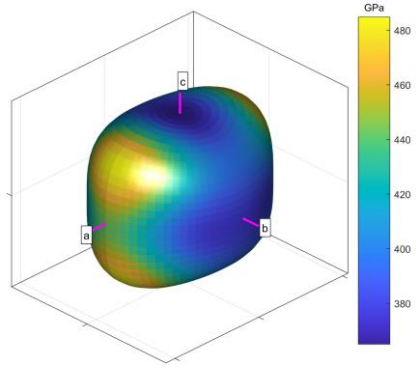

$AlCr_2B_2$

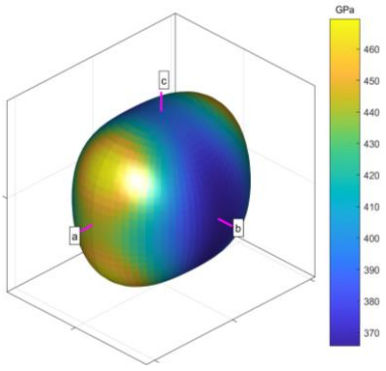

$AlCrMnB_2$

Figure 2. Three-dimensional representations of the direction-dependent Young's moduli for $AlCr_2B_2$ and $AlCrMnB_2$.
Şekil 2. $AlCr_2B_2$ ve $AlCrMnB_2$ için yön bağımlı Young modüllerinin üç boyutlu temsilleri.

Two-dimensional representations of Young's moduli for borides on the (100), (010), and (001) planes show circular curves for isotropic crystalline materials, with increased deviation indicating higher degrees of anisotropy (Zhu et al., 2019). When we analyze the two-dimensional representations of Young's moduli of the borides on the (100), (010), and (001) planes, it is observed that in $AlCr_2B_2$, compared to $AlCrMnB_2$, there is a greater deviation in circularity in the (010) and (001) planes. Therefore, on the (010) and (001) planes, $AlCr_2B_2$ shows a higher anisotropy of Young's moduli compared to $AlCrMnB_2$. Conversely, there is a lesser deviation from circularity in the (100) plane. Thus, on the (100) plane, $AlCrMnB_2$ exhibits slightly more deviation in Young's moduli compared to $AlCr_2B_2$, indicating a higher degree of anisotropy.

Two-dimensional representations of Young's moduli for borides on the (100), (010), and (001) planes are shown in Figure 3.

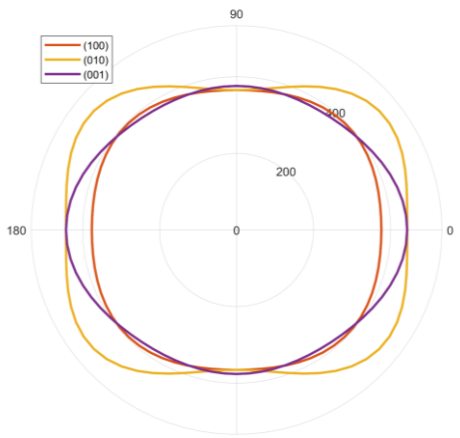

$AlCr_2B_2$

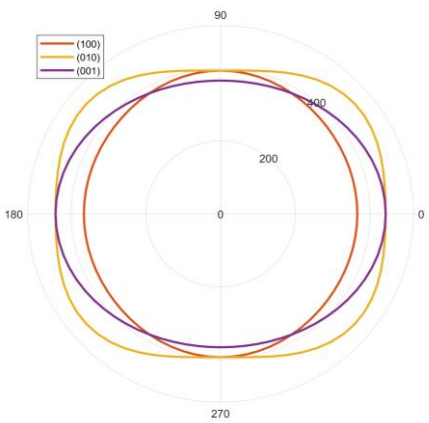

$AlCrMnB_2$

Figure 3. Two-dimensional representations of the Young's moduli of $AlCr_2B_2$ and $AlCrMnB_2$ in the (100), (010), and (001) planes.
Şekil 3. $AlCr_2B_2$ ve $AlCrMnB_2$'nin (100), (010) ve (001) düzlemlerindeki Young modüllerinin iki boyutlu temsilleri.

4. Conclusion

In this study, we utilized the CASTEP code and employed first-principles calculations within the framework of Density Functional Theory (DFT) to analyze the mechanical properties of $AlCr_2B_2$ and $AlCrMnB_2$. The results show that $AlCr_2B_2$ and $AlCrMnB_2$ are mechanically stable. In both borides, the C_{11} value is greater than the C_{22} and C_{33} values; therefore, it is expected that the borides will exhibit greater resistance to compression along the a-axis compared to the b and c-axes. Therefore, it is thought that strong B-B bonds will be present along the a-axis in all crystals. The obtained elastic constants, bulk modulus, shear modulus, Young's modulus, Poisson's ratio, Pugh's ratio, theoretical Vickers hardness, elastic Debye temperature, Cauchy pressures, and elastic anisotropy indices (A_1, A_2, A_3, A_B, A_G, A^U) for $AlCr_2B_2$ have exhibited a strong agreement with other computational results. In the $AlCr_2B_2$, the addition of the Mn element instead of the reduced Cr has led to a decrease in elastic moduli (bulk, shear, and Young's modulus), theoretical Vickers hardness, elastic Debye temperature, and elastic anisotropy. In addition, it has been observed that the Poisson ratio remains unchanged, and the Pugh ratio has increased by a very small amount (0.01). Due to the slight increase in the Pugh ratio, it is believed that there will be a slight decrease in brittleness as well. It has been observed that $AlCr_2B_2$ deviates more from sphericity compared to $AlCrMnB_2$, and this phenomenon has been attributed to the difference in the C_{11} and C_{33} elastic constants, with the (C_{11}-C_{33}) value in $AlCrB_2$ (82.2) being larger than that in $AlCrMnB_2$ (50.7).

5. Conflicts of Interest

The authors declare no conflict of interest.

6. References

Ali, M. M., Hadi, M. A., Rahman, M. L., Haque, F. H., Haider, A. F. M. Y., & Aftabuzzaman, M. (2020). DFT investigations into the physical properties of a MAB phase Cr4AlB4. *Journal of Alloys and Compounds*, 821, 153547.

Aydin, S., & Şimşek, M. (2020). Pressure-induced magnetic phase transitions of intermetallic Fe2AlB2. *Journal of Magnetism and Magnetic Materials*, 502, 166453.

Chai, P., Stoian, S. A., Tan, X., Dube, P. A., & Shatruk, M. (2015). Investigation of magnetic properties and electronic structure of layered-structure borides AlT2B2 (T= Fe, Mn, Cr) and AlFe2–xMnxB2. *Journal of Solid State Chemistry*, 224, 52-61.

Clark, S. J., Segall, M. D., Pickard, C. J., Hasnip, P. J., Probert, M. I., Refson, K., & Payne, M. C. (2005). First principles methods using CASTEP. *Zeitschrift für kristallographie-crystalline materials*, 220(5-6), 567-570.

Han, L., Wang, S., Zhu, J., Han, S., Li, W., Chen, B., ... & Jin, C. (2015). Hardness, elastic, and electronic properties of chromium monoboride. *Applied Physics Letters*, 106(22).

Healy, D. (2023) Davehealy-github/AnisoVis: Visualisation of Anisotropy, GitHub. Retrieved from: https://github.com/DaveHealy-github/AnisoVis

Kádas, K., Luşan, D., Hellsvik, J., Cedervall, J., Berastegui, P., Sahlberg, M., ... & Eriksson, O. (2017). AlM2B2 (M= Cr, Mn, Fe, Co, Ni): a group of nanolaminated materials. *Journal of Physics: Condensed Matter*, 29(15), 155402.

Kota, S., Sokol, M., & Barsoum, M. W. (2020). A progress report on the MAB phases: atomically laminated, ternary transition metal borides. *International Materials Reviews*, 65(4), 226-255.

Li, X. H., Cui, H. L., & Zhang, R. Z. (2018). Structural, optical, and thermal properties of MAX-phase Cr 2 AlB 2. *Frontiers of Physics*, 13, 1-9.

Lu, J., Kota, S., Barsoum, M. W., & Hultman, L. (2017). Atomic structure and lattice defects in nanolaminated ternary transition metal borides. *Materials Research Letters*, 5(4), 235-241.

Momma, K., & Izumi, F. (2011). VESTA 3 for three-dimensional visualization of crystal, volumetric and morphology data. *Journal of applied crystallography*, 44(6), 1272-1276.

Monkhorst, H. J., & Pack, J. D. (1976). Special points for Brillouin-zone integrations. *Physical review B*, 13(12), 5188.

Natu, V., Kota, S. S., & Barsoum, M. W. (2020). X-ray photoelectron spectroscopy of the MAB phases, MoAlB, M2AlB2 (M= Cr, Fe), Cr3AlB4 and their binary monoborides. *Journal of the European Ceramic Society*, 40(2), 305-314.

Nie, L., Zhou, W., & Zhan, Y. (2013). Theoretical investigation of the Al–Cr–B orthorhombic ternary compounds. *Computational and Theoretical Chemistry*, 1020, 51-56.

Peng, M., Wang, R., Wu, Y., Yang, A., & Duan, Y. (2022). Elastic anisotropies, thermal conductivities and tensile properties of MAX phases Zr2AlC and Zr2AlN: A first-principles calculation. *Vacuum*, 196, 110715.

Verger, L., Kota, S., Roussel, H., Ouisse, T., & Barsoum, M. W. (2018). Anisotropic thermal expansions of select layered ternary transition metal borides: MoAlB, Cr2AlB2, Mn2AlB2, and Fe2AlB2. *Journal of Applied Physics*, 124(20).

Wang, P., Kumar, R., Sankaran, E. M., Qi, X., Zhang, X., Popov, D., ... & Wang, L. (2018). Vanadium diboride (VB2) synthesized at high pressure: elastic, mechanical, electronic, and magnetic properties and thermal stability. *Inorganic chemistry*, 57(3), 1096-1105.

Wang, R., Tao, X., Ouyang, Y., Chen, H., & Peng, Q. (2020). Suggest a new approach to fabricate AlFe2B2. *Computational Materials Science*, 171, 109239.

Zhu, S., Zhang, X., Chen, J., Liu, C., Li, D., Yu, H., & Wang, F. (2019). Insight into the elastic, electronic properties, anisotropy in elasticity of Manganese Borides. *Vacuum*, 165, 118-126.